Hindawi
Advances in Polymer Technology
Volume 2020, Article ID 3161068, 15 pages
https://doi.org/10.1155/2020/3161068

Research Article

Microstructure, Tensile Property, and Surface Quality of Glass Fiber-Reinforced Polypropylene Parts Molded by Rapid Heat Cycle Molding

Feng Liu,[1,2] **Taidong Li**,[1] **Fuyu Xu**,[1] **Jiquan Li**,[1] **and Shaofei Jiang**[1]

[1]*College of Mechanical Engineering, Zhejiang University of Technology, Hangzhou 310014, China*
[2]*School of Mechanical and Automotive Engineering, Zhejiang University of Water Resources and Electric Power, Hangzhou 310018, China*

Correspondence should be addressed to Shaofei Jiang; jsf75@zjut.edu.cn

Received 26 July 2019; Revised 7 September 2019; Accepted 17 September 2019; Published 26 March 2020

Academic Editor: Huamin Zhou

The microstructure of a molded product considerably influences its macroscopic properties. In this study, the influence of molding process on microstructure, tensile property, and surface quality was explored on the glass fiber-reinforced polypropylene (GFRPP) parts molded by rapid heat cycle molding (RHCM) and conversion injection molding (CIM). Tensile strength and surface gloss were chosen to measure macroscopic properties of the molded parts. The microstructure including multilayer, fiber orientation, crystallinity, and fiber-matrix bonding strength were analyzed by simulations, scanning electron microscopy, wide-angle X-ray diffraction, and dynamic mechanical analysis. The relationship between the macroscopic properties and microstructure of the RHCM samples was also discussed. The results indicate that as the mold cavity surface temperature increases, the tensile strength increases firstly and decreases thereafter. The tensile strength of RHCM parts reached the maximum at the mold heating temperature of 60°C. It is also observed that the surface gloss of the sample increases as the mold cavity surface temperature rises, and the increase of surface gloss decreases distinctly with the mold heating temperature higher than 90°C.

1. Introduction

Short glass fiber-reinforced polypropylene (GFRPP) composites are recyclable materials with good mechanical properties, high chemical resistance, excellent thermal stability, and attractive performance-cost ratio. In view of these advantages, the GFRPP is widely used in structural applications in the fields of aerospace, automotive, civil, and marine engineering [1–5]. It is well known that the macroscopic performance of the product is substantially dependent on its microstructure [6–8]. In the past, considerable efforts have been devoted to adapt the microstructures of GFRPP products and improve their macroscopic performance [9–15]. It is presumed that the mechanical properties of GFRPP products significantly depend on the combined effects of glass fiber orientation and distribution, fiber-matrix interface bonding strength conditions, and state of matrix crystallization, while some surface defects, such as flow marks, floating fibers, weld lines, and jetting marks cannot be avoided through the CIM process [16, 17]. The rapid heat cycle molding (RHCM) process is a relatively new technique that can not only significantly reduce or even eliminate surface defects but also significantly shorten the production cycle and reduce energy consumption and environmental pollution [18]. The most evident difference between the RHCM and CIM processes is that the former employs dynamic mold temperature control technology whereby the mold temperature is rapidly increased to a preset temperature before the mold is filled with the melt. During the filling and packing stage, high temperature is maintained; thereafter, the melt is quickly cooled to demold it before proceeding to the next stage of the production cycle [19–21]. Thus, the RHCM process has a more complex thermomechanical history than the CIM process [22].

To date the research works on the relationship between microstructure and macroscopic properties of products molded by the RHCM process have received increasing attention. Wang et al. [23] investigated the effect of mold cavity surface temperature in the filling process on the crystallization state of virgin PP in injected plastic part layers with different thicknesses. They also explored the relationship between the surface quality of plastic parts, crystallinity, and residual stress in the RHCM. Recently, Speranza et al. [24] reported that the mold surface temperature markedly influenced the molecular orientation and morphology developed in injection-molded samples, and the combination of flow fields and cooling rate experienced by the virgin polymer determined the multilayer structure of samples. Under strong flow field and high temperature conditions, a tightly packed structure (called shish-kebab) aligned along the flow direction was observed, whereas the formation of β-phase in cylindrite form was observed in weak flow fields. Li et al. [22] proposed a novel method to acquire the crystallization evolution information of virgin polymers during the RHCM process. The influence of temperature and shear rate on crystallization was considered in this method, thereby the method was beneficial to the optimization of the RHCM molding process for the manufacture of high-quality products. Liparoti et al. [25] analyzed the effect of the operative conditions of injection molding process on the morphology distribution inside molded products and found that the shear layer thickness was reduced in samples produced at high mold temperatures. It was particularly noted that the shear layer disappeared when the packing pressure and heating time were 360 bar and 20 s, respectively.

Based on the foregoing investigations, literature studies are mainly focused on the virgin polymer. So far, limited research works are about short glass fiber-reinforced polymer under the RHCM process. Li et al. [9] established a novel model describing the confluent process for the fiber-reinforced melt in the RHCM and described the relationship between the mold temperature and appearance of the confluent region. Furthermore, they presented the effect of fiber orientation in the confluent region on the impact strength of resultant parts. Wang et al. [26] used two reinforced plastics including ABS/PMMA/nano-$CaCO_3$ and 20% fiber-reinforced polypropylene to investigate the influence of cavity surface temperature immediately before filling on the surface appearance and texture of the molded reinforced plastic parts using the RHCM. The roughness, gloss, and morphology of the surface are characterized with white light interferometer, gloss meter, and optical microscope, respectively. They found that the mold surface temperature immediately before filling has a significant influence on the surface appearance of the molded part. In another work, the same research group [27] found that for fiber-reinforced plastics of PP + 20% glass fiber produced through the RHCM, the cavity surface temperature set to 118°C at the filling stage reduced the tensile strength of the part without a weld mark but slightly increased that of the part with a weld mark.

The aforementioned studies indicate that the microstructure (e.g., multilayer structure, fiber orientation, state of crystallization, interfacial bonding strength, and surface morphology) and macroperformance (e.g., tensile strength and surface gloss) of GFRPP product molded by RHCM have not been established. This makes the processing and parameter adjustment of the RHCM have great blindness. Hence, it is crucial to obtain the microstructure evolution law of reinforced thermoplastics produced by the RHCM process to reveal the mapping relationship between the macroscopic properties and microstructure of RHCM products. In this study, an electric heating RHCM is employed to understand the different cavity surface temperature action mechanisms that regulate the tensile strength and the surface appearance quality of a reinforced polymer product without a weld line. The macroscopic properties and microstructure are tested and analyzed by scanning electronic microscope (SEM), wide-angle X-ray diffraction (WAXRD), dynamic thermomechanical analysis (DMA), Autodesk Moldflow™, surface roughness meter, and surface gloss meter. The corelationships between the macroscopic properties, microstructure, and processing of RHCM products are explored.

2. Materials and Methods

2.1. Materials. The testing material adopted in this study is PP with 30% short glass fibers (supplied by Suzhou Yulian Engineering Plastics Co. Ltd., China) with a density of 1.18 g/cm^3 (ASTM D792), melt flow rate of 1.8 g/10 min (ASTM: D1238), and heat deflection temperature of 140°C (ASTM: D648).

2.2. Experimental Setup and Procedure. The employed electric heating RHCM apparatus (Figure 1 [28]) is mainly composed of electric heating rods, K-type thermocouple sensor, and mold temperature controller MTS-32II system (Beijing CHN-TOP Machinery Group Co. Ltd., China) to measure, regulate, and display the mold surface heating temperature, and a two-plate RHCM mold (the cavity surface is polished to achieve a glossy mirror surface with a roughness Ra of about 57 nm). Electrical heating rods are only deployed at the fixed side of the mold to heat this side rapidly before filling. The regular water-cooling tunnels are used to cool both movable and fixed sides of the mold with turbulent room temperature cooling water after the packing stage. An injection molding machine (HTFX5 series, Haitian Plastic Machinery Group Co. Ltd., China) is used. All process parameters are listed in Table 1.

And only the samples produced after stabilizing the process parameters are used. For each set of molding conditions, no less than five samples are employed for the subsequent measurements and analysis.

2.3. Specimen Preparation. The sample position is selected as shown in Figure 2. To facilitate description, the samples molded with cavity surface temperatures of 60, 90, and 120°C are designated as RHCM60, RHCM90, and RHCM120, respectively. All of the RHCM test samples are selected and processed on the side of the fixed half mold. The injection-

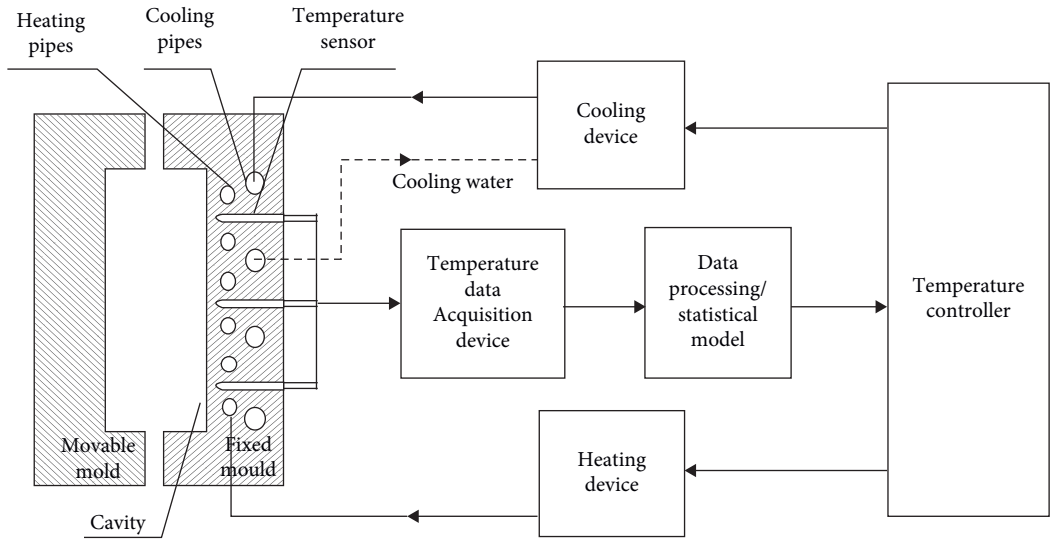

Figure 1: Schematic diagram of RHCM apparatus [32].

Table 1: Processing parameters used in RHCM tests.

Melt temperature (°C)	Injection pressure (MPa)	Injection velocity (%)	Packing time (s)	Packing pressure (MPa)	Mold heating temperature (°C)	Cooling time (s)
240	60	45	9	50	60/90/120	30

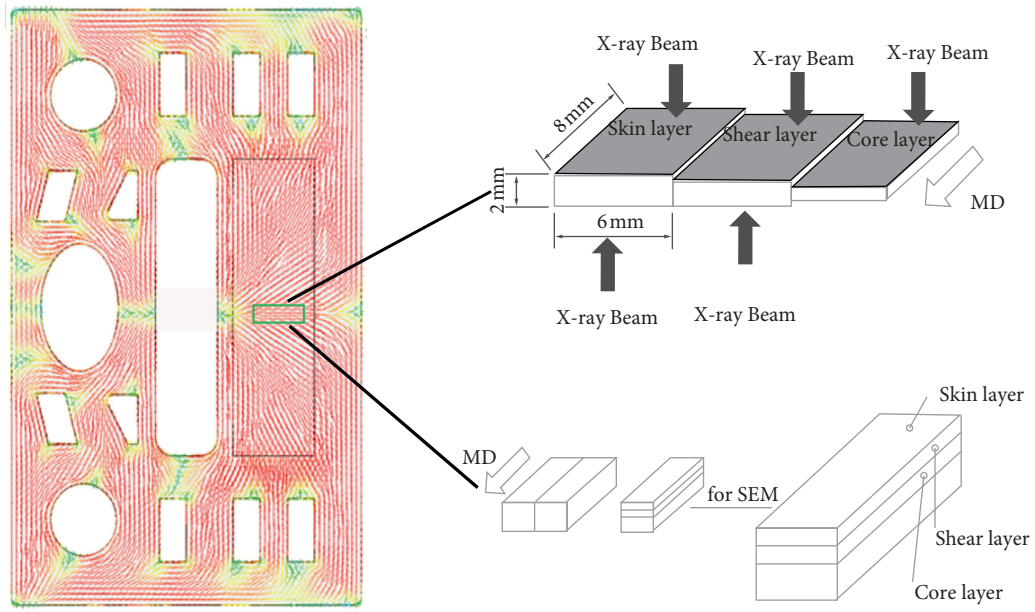

Figure 2: Schematic of parts and locations of tested samples.

molded samples are placed in liquid nitrogen and thereafter fractured as illustrated in Figure 2.

2.4. Performance Testing. According to ASTM D638, tensile tests are conducted on a universal testing instrument (INSTRON-8872, USA). The sample surface roughness is measured by a roughness meter (Mitutoyo SJ-410, Japan). The sample surface gloss is measured according to ASTM D523 using a gloss meter (WGG-60, Tongfu Electromechanical Equipment Co., Ltd., China).

2.5. Microstructure Analysis. All fractured surfaces for examination are polished in sequence using metallographic sandpaper with particle sizes of 300#, 600#, and 1500# on a grinding and polishing machine. The polished cross section is sputtered with gold in a vacuum; thereafter, the

microstructure of the sample is observed with a scanning electron microscope (Hitachi S-4700, Japan). The scanning voltage is 15.0 kV, and a total magnification of 150X is applied. The WAXRD technique is employed to estimate the crystallinity in each specified layer across the sample thickness. The sample position is specifically selected along the thickness, as illustrated in Figure 2. The WAXD is performed with an X'Pert PRO X-ray diffraction instrument (PANalytical B.V., Almelo, Netherlands) with a Cu Kα source and an average wavelength of 0.154056 nm. The equipment is operated at 40 kV and 40 mA in ambient temperature with a diffraction angle (2θ) range of 10°–40° and a 2°/min scan rate. The interfacial bonding strength of GFRPP composites can be characterized by the DMA test using DMAQ800 (TA instruments, America). Rectangular test samples (each 3 mm × 1 mm × 2 mm) are heated from −20 to 40°C at a rate of 2°C/min. The single cantilever mode is employed to test the samples at an oscillation amplitude and frequency of 10 μm and 1 Hz, respectively.

Autodesk Moldflow™ is utilized to evaluate the glass fiber orientation distribution in the sample thickness direction. In the simulation, the material properties and corresponding boundary conditions are set according to the parameters used in the actual CIM and RHCM experiments.

3. Results and Discussion

3.1. Effect of RHCM Process on Multilayer Microstructure of GFRPP. The SEM micrographs of multilayer structures are shown in Figure 3, which appear in the cross sections of CIM and RHCM60 samples. In the cross section of samples, the CIM sample exhibits a distinct symmetric skin-shear-core structure, whereas RHCM samples present an asymmetric multilayer structure. The layers thicknesses on the fixed mold side are considerably different from those on the movable mold side. This asymmetric structure is mainly attributed to the heating of the cavity surface in the fixed half mold with dynamic mold temperature control technology, and it well demonstrates the effect of different heating temperatures on the microstructures of RHCM samples. Figure 4 exhibits the skin layer thickness variation trends in RHCM and CIM samples produced at different cavity surface temperatures before filling. Based on the SEM images of specimen cross sections, the thickness of multilayers is determined by taking the average of multiple measurements with the aid of JMICROVISION software.

Figure 5(a) shows that the skin layer thickness of the sample decreases as the cavity temperature before filling increases, and such a decreasing tendency can be interpreted as temperature gradient distribution. Compared with the RHCM process, the CIM process has the largest temperature gradient between the melt and the cavity surface; hence, the entering melt rapidly cools upon contact with the cold cavity surface and immediately condenses and forms the skin layer, and accordingly, the CIM sample has the thickest skin layer. With the increase of temperature, the temperature gradient decreases. According to the foregoing, it is not difficult to sort the skin layer thickness in descending order as the cavity temperature before filling increases.

In Figure 5(b), the shear layer thickness in all RHCM samples is thicker than the shear layer thickness in the CIM sample. According to the previous analysis, the CIM process produces the thickest skin layer. Evidently, this skin layer provides the best heat insulation effect for the melt and weakens the heat exchange between the melt and mold wall and thereafter decreases the temperature gradient below the CIM skin layer; as a result, the shear layer thickness in the CIM sample is the thinnest. Compared with CIM sample, as the cavity surface temperature further increases, the skin layer thermal insulation performance further weakens and the shear layer thickness of the RHCM samples presents a descending order.

In Figure 5(c), it can be observed that the core layer thickness in the RHCM samples increases with the increase in the cavity surface temperature, and the core layer thickness in the CIM sample is thicker than that in the RHCM samples processed at cavity surface temperatures of 60 and 90°C. This phenomenon can be attributed to the fact that the thicker skin layer in the CIM sample has a good heat insulation effect, the temperature gradient in the melt under the skin layer is smaller, and consequently, the core layer thickness in the CIM sample is relatively thicker. In the RHCM process, the temperature difference between the cavity surface and melt gradually decreases with the increase in the cavity surface temperature; this explains the gradual increase in the core layer thickness. When the cavity surface temperature rises to 120°C, the core layer reaches its maximum thickness.

3.2. Effect of RHCM Process on Fiber Orientation in the GFRPP Microstructure. The model is constructed using tetrahedral elements with 11 layers meshed in the thickness direction. Figure 6 shows the meshed model established with the software. The fiber orientation distribution in different layers on the side of the fixed half mold is obtained by Moldflow™ simulation, as shown in Figure 7.

In the CIM process, the shear layer has the highest fiber-reinforced orientation parallel to the flow direction, followed by the skin layer. In the core layer, the fibers are observed to be oriented randomly. These results confirm those reported in literature [6, 29, 30]. Figure 7(a) shows the skin layer fiber orientation tensors obtained at different cavity surface temperatures. As the cavity surface temperature increases, the cooling and freezing rates of the skin layer are slowed down. These afford ample time for the fibers to be oriented in the flow direction as well as more time for the molecular orientation to relax. Under this condition, both shearing and stretching coupled with the molecular orientation effect are strengthened. These factors have opposite effects on the skin layer fiber orientation, and the final fiber orientation results are determined by these two competing effects. For RHCM60, the shearing and stretching effects are more predominant in the skin layer fiber orientation; accordingly, this sample has a relatively higher skin layer fiber orientation than the CIM sample. On the other hand, because the melt cooling rate in RHCM90 is lower than that in RHCM60, the skin layer is in a high elastic state over a longer period. The

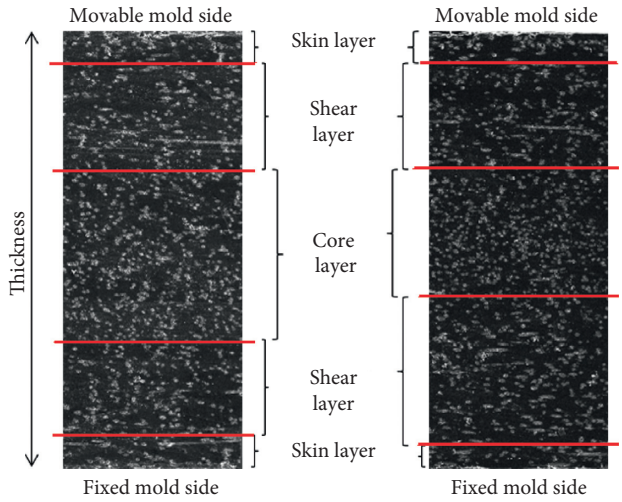

Figure 3: SEM micrographs of inner multilayer thickness distribution. Trend of tested samples: (a) CIM sample; (b) RHCM sample.

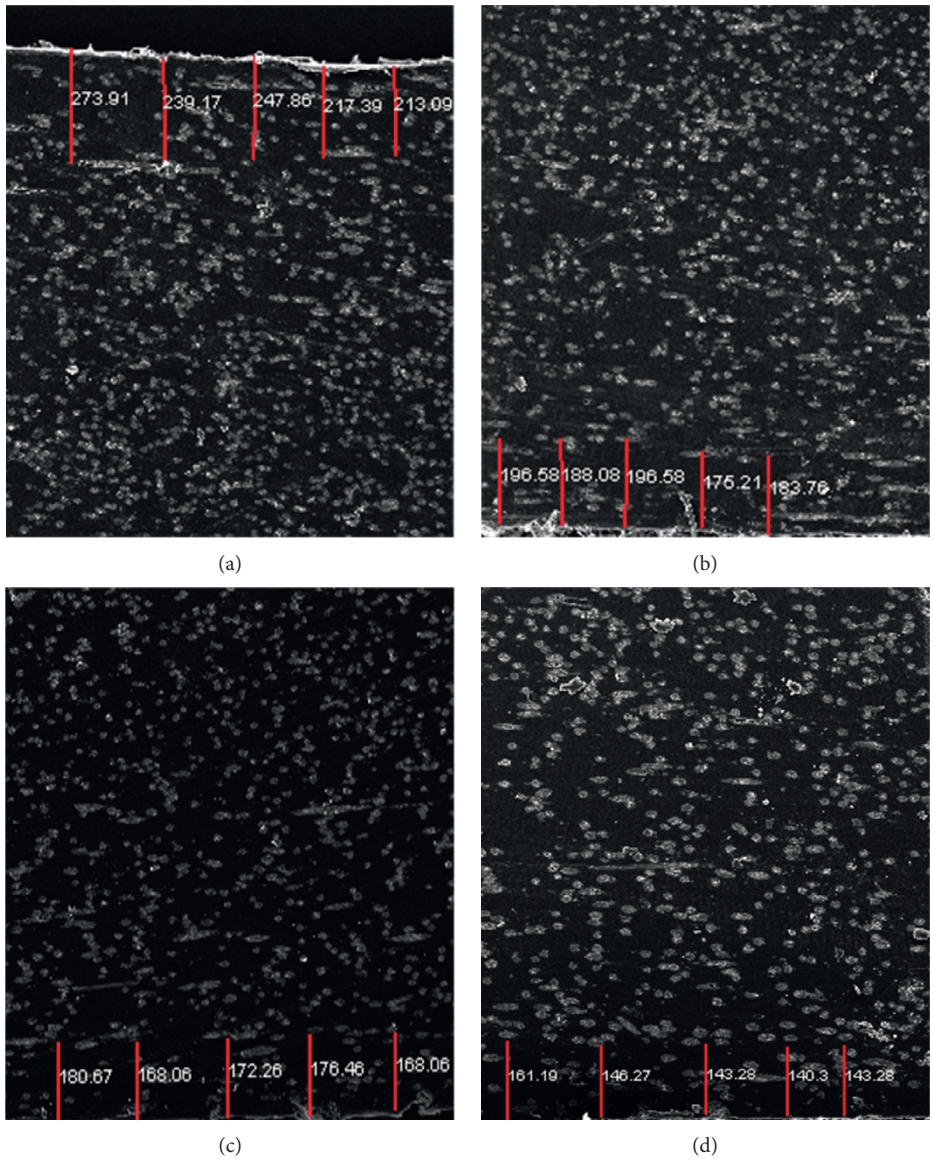

Figure 4: SEM micrographs of skin layer thickness in RHCM and CIM samples produced at different cavity surface temperatures before filling: (a) CIM; (b) RHCM60; (c) RHCM90; (d) RHCM120 (unit: μm).

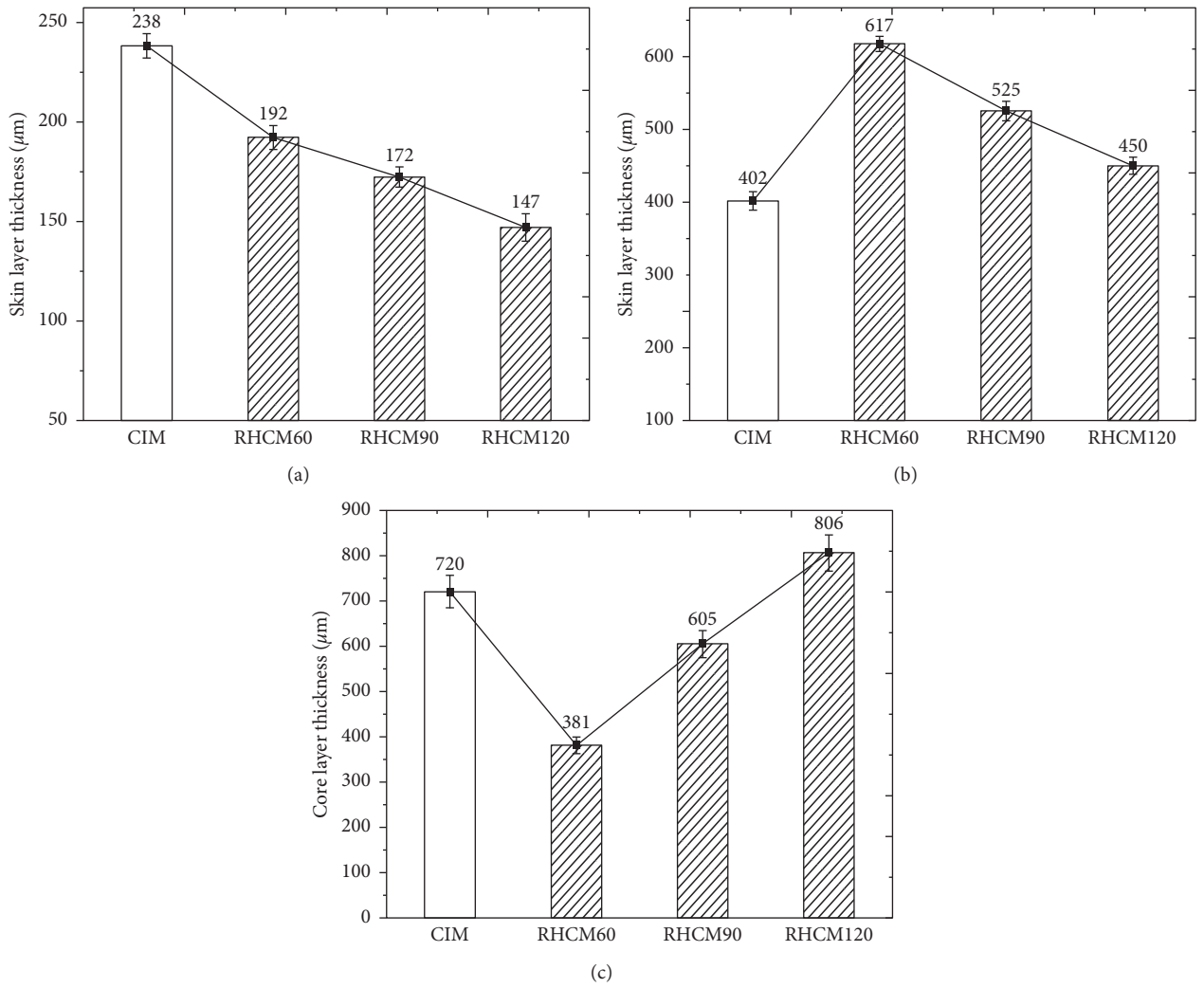

FIGURE 5: Schematic of each layer thickness change trend in RHCM and CIM samples: (a) skin layer thickness; (b) shear layer thickness; (c) core layer thickness.

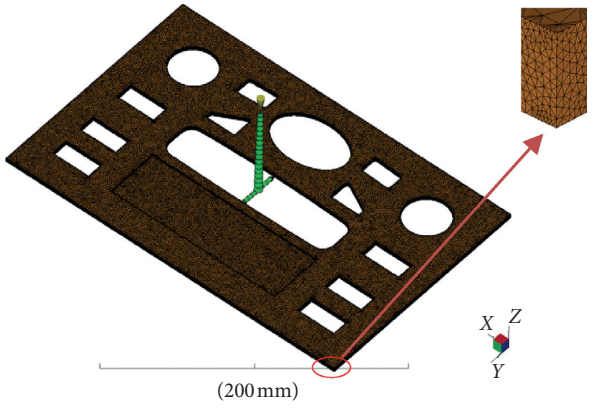

FIGURE 6: Schematic of the simulation model.

shearing and stretching effects are weaker because the velocity gradient is further reduced under this condition, and the internal fibers undergo a certain random movement based on the high temperature relaxation effect of the oriented polymer macromolecular chains. All of the these allow RHCM90 sample to have a relatively lower skin layer fiber orientation than the CIM sample. In the RHCM120 process, the cooling rate is the slowest, the oriented molecular chain relaxation is the most sufficient, and the skin layer fiber orientation is basically unoriented.

Figure 7(b) shows the fiber orientation tensor of the shear layer in the RHCM samples. It can be observed that RHCM60 sample has the highest shear layer fiber orientation. In the RHCM process, the melt in the shear layer is subjected to a lower shearing force compared with that experienced in the skin layer. However, the shear action time is longer, and the inner fibers have sufficient time to be oriented. Hence, the degree of fiber orientation in the shear layer is relatively higher than that in the skin layer. Moreover, notice that the fiber orientation tensor in the shear layer decreases drastically with the increase in mold temperature. Recall that as the heating temperature of the mold increases, the temperature gradient in the melt decreases; this causes the flow velocity difference among the layers to

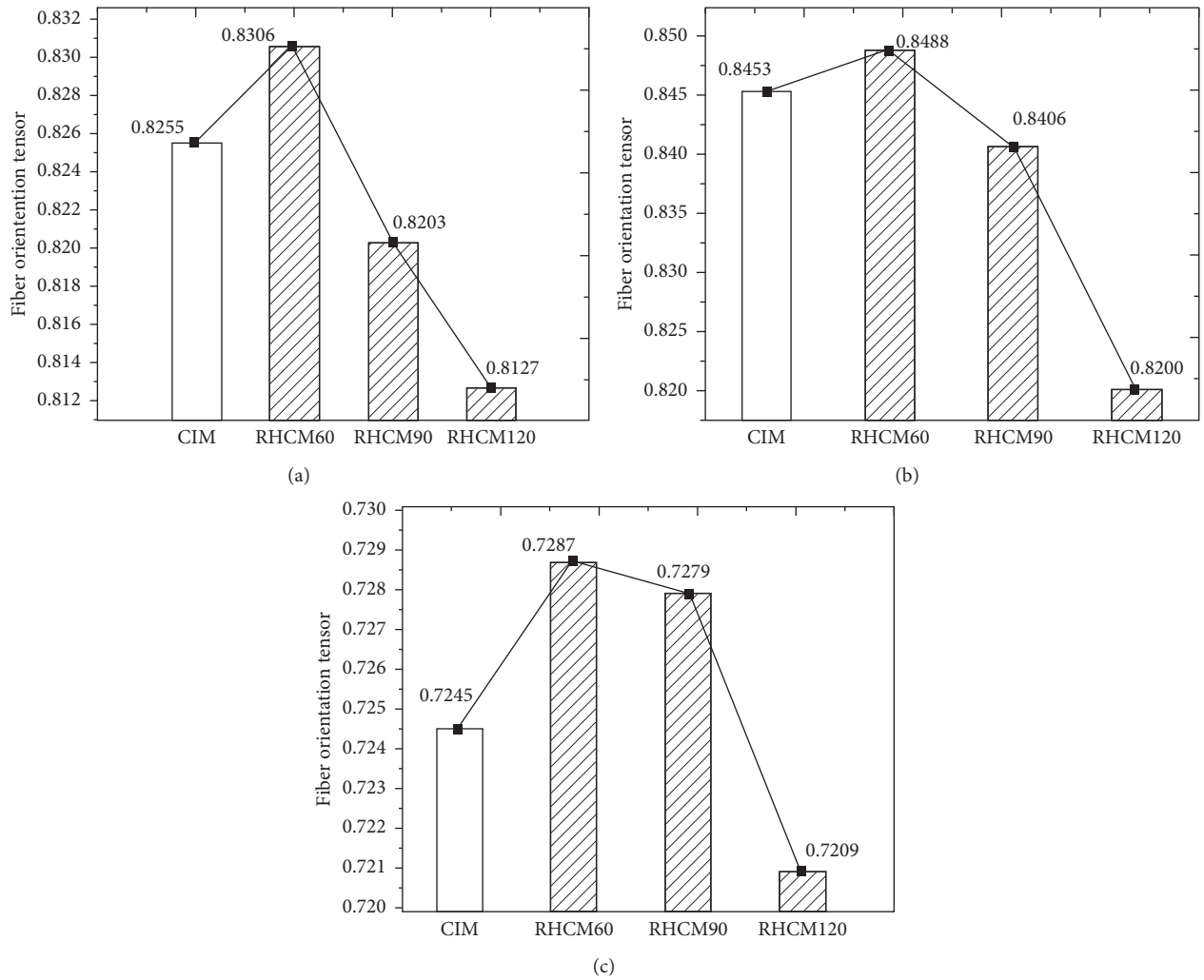

Figure 7: Schematic of layer fiber orientation tensor change trend in RHCM and CIM samples: (a) within skin layer; (b) within shear layer; (c) within core layer.

decrease. Thereafter, the shearing effect among the layers is weakened, particularly in RHCM120 sample. Figure 7(c) shows the core layer fiber orientation tensor of samples. In general, the core layer fiber orientation in all RHCM and CIM samples is relatively low. Compared with the skin and shear layers, the core layer has a uniform temperature distribution and a melt temperature that can be maintained higher than the glass transition temperature in both RHCM and CIM processes. Moreover, it has practically no shearing effect that can impact its fibers, and its polymer molecules have sufficient time to relax. Accordingly, with its fibers freely oriented, the core layer has a low fiber orientation.

3.3. Effect of RHCM Process on Crystallinity in the Microstructure of GFRPP. The statistical results of crystallinity in each layer in all samples are shown in Figure 8. The inner crystallization variation trend in the CIM sample is the same as the study result obtained by Salah et al. [31]. And the

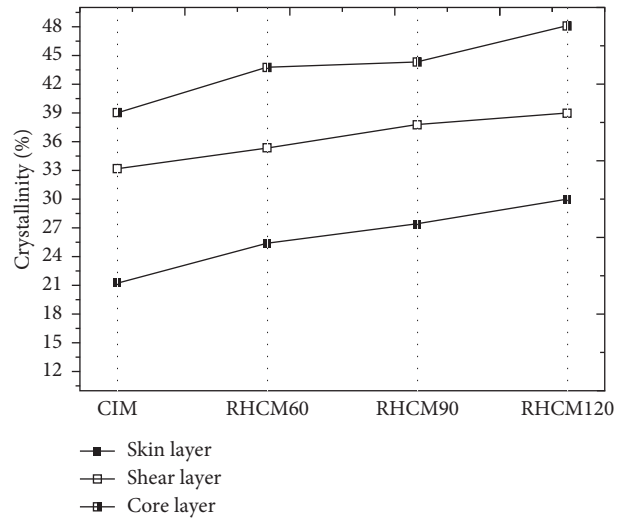

Figure 8: Statistical results of crystallinity in each layer in CIM and RHCM samples.

crystallinity in each layer in the RHCM samples is higher than that in the CIM sample; furthermore, the crystallinity in all layers increases continuously as the cavity surface temperature increases. In the RHCM process, when the melt comes into contact with the cavity surface having a higher temperature, the melt experiences a temperature range that is suitable for crystallization. And it is widely known that good fluidity results in less pressure loss in the melt flow direction and enhances the subsequent packing effects and, hence, decreases the free volume in the melt and increases the melt density; thereafter, the orientation of the molecular chains formed in the filling stage is further strengthened during the subsequent packing stage, and all these factors facilitate crystallization.

Additionally, it is found that the crystallinity in all layers increases continuously as the cavity surface temperature increases, the core layer has a higher crystallinity than the shear layer, and the skin layer has the lowest crystallinity. The heat exchange between the melt and the mold cavity surface is weakened because of the skin layer's heat insulation effect, at the same time the temperature in the shear layer is higher than that in the skin layer, and the crystallization time is relatively longer. And the intensive shear stress field in the shear layer triggers shear-induced crystallization. Thus, it can be concluded that as the heating temperature of the mold increases, both crystallization rate and crystallization time increase, and the crystallinity in shear layer is higher than that in skin layer. Additionally, both skin and shear layers act as insulating layers to further reduce the heat exchange between the mold surface and core layer; the core layer has a relatively longer and better crystallization time and zone. Thus, the core layer in each sample has the highest crystallinity, followed by the shear layer and skin layer in sequence.

3.4. Effect of RHCM Process on Fiber-Matrix Bonding Strength of GFRPP Composites. The interfacial bonding strength determines the stress transfer between the reinforcing fiber and matrix and is recognized as the key factor in the global mechanical performance of composites [10, 12, 32, 33]. To estimate the interfacial bonding strength of GFRPP composites under different mold cavity surface temperatures, the DMA test is employed [34]. The damping factor (tan δ) curves indicate the interfacial bonding strength of GFRPP composites, as shown in Figure 9.

As the mold cavity surface temperature increases, the peak of the mechanical loss in the sample gradually decreases, which indicates that the bonding strength between the reinforcing fiber and PP matrix increases as the temperature increases. It can be explained as follows: the global crystallinity in the sample increases under this condition, which causes the crystal area to expend, and the free movement volume of the molecular chain to reduce; these factors limit the movement of polymer molecular chains. Hence, the friction between molecular chains and fibers is decreased, and the sample's mechanical loss (tan δ) peak gradually decreases. Accordingly, the fiber-matrix bonding strength increases gradually with the increase of cavity surface temperature.

3.5. Relationship between Microstructure and Tensile Property. Figure 10 shows the tensile strength of samples produced by different CIM and RHCM processes. RHCM60 sample has the highest tensile strength, which reaches 57.61 MPa; this indicates that the RHCM process effectively improves the tensile property of the GFRPP composites. However, it is also found that as the mold cavity temperature before filling increases, the tensile strength of the RHCM sample gradually decreases, and even the tensile strength of RHCM120 sample is lower than that of the CIM sample. The tensile strength difference can be illustrated by the microstructure of the molded samples.

Figure 11 shows the microstructure comparison of RHCM60 and CIM samples. It is observed that the shear layer thicknesses with highly oriented fibers of RHCM60 increase by 53.5% compared with the CIM sample. However, the thicknesses of the skin and core layers, with the relatively lower fiber orientation tensors, are reduced by approximately 19.3% and 47.1%, respectively. Meanwhile, both crystallinity and fiber orientation in each layer in RHCM60 are higher than those in the CIM sample. The crystallinity in the skin, shear, and core layers increased by 19.4%, 6.5%, and 12.1%, respectively. Thus, the overall crystallinity and fiber orientation of RHCM60 in the cross section are higher than those in the CIM sample. When the external force exerts a tensile load on the sample, the increase in fiber orientation causes more fibers to bear the load transmitted by the substrate. The increase in matrix crystallinity indicates that the contact area between the crystal and amorphous regions increases; this also aids in the loads transfer from the matrix to the fiber. Hence, the tensile strength of RHCM60 is higher than that of the CIM sample.

It is evident in Figure 12 that as the cavity temperature is increased, the thicknesses of the skin and shear layers with higher fiber orientations are considerably reduced with decrements of 10.4%, 14.5%, and 14.9%, 14.3%, respectively. The thickness of the core layer with low fiber orientation is increased significantly with increments of 58.8% and 33.2%. Hence, as the cavity surface temperature is increased, the overall fiber orientation in the thickness direction of the sample is drastically lowered. Moreover, the crystallinity in each layer has different degrees of increment, ranging from 1.3% to 9.4%; the overall crystallinity in the RHCM samples increases continuously as the temperature increases. Although the high crystallinity matrix under this condition is advantageous for sustaining more applied loads, it is presumed that the effect of drastic reduction in the thickness of the shear layer with high fiber orientation on the tensile strength is more distinct.

3.6. Relationship between Microstructure and Surface Gloss. As shown in Figure 13, the RHCM process can effectively and continuously improve the surface gloss of the sample from 37.5 to 78.8 Gs as the surface temperature rises. The sample surface gloss is determined by the surface morphology of the product.

Table 2 summarizes the surface roughness measurement result of each sample. It indicates that the surface roughness

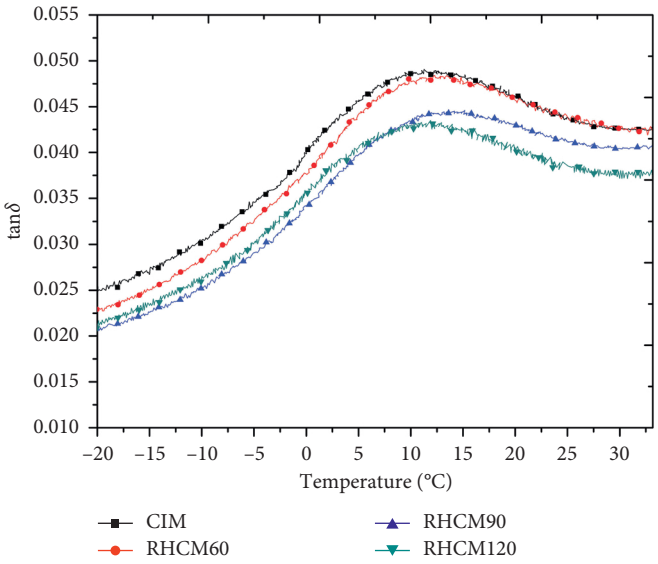

Figure 9: Mechanical loss (tan δ) curve of RHCM and CIM samples.

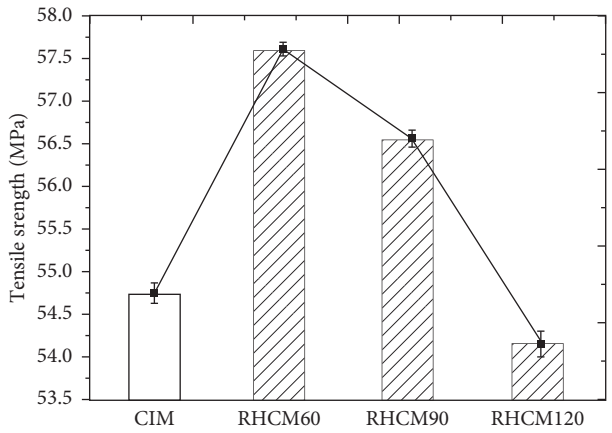

Figure 10: Tensile strength of RHCM and CIM samples.

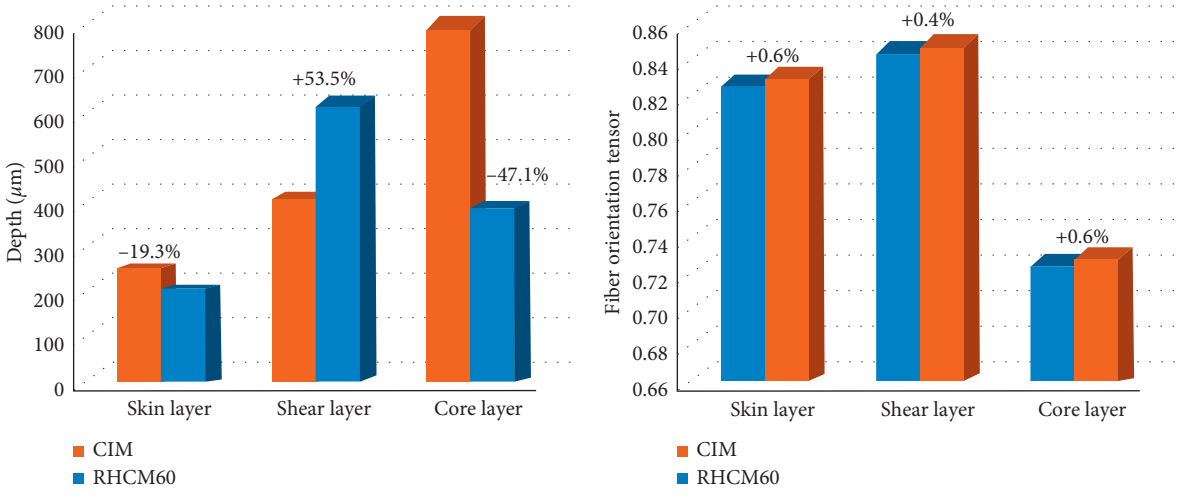

Figure 11: Continued.

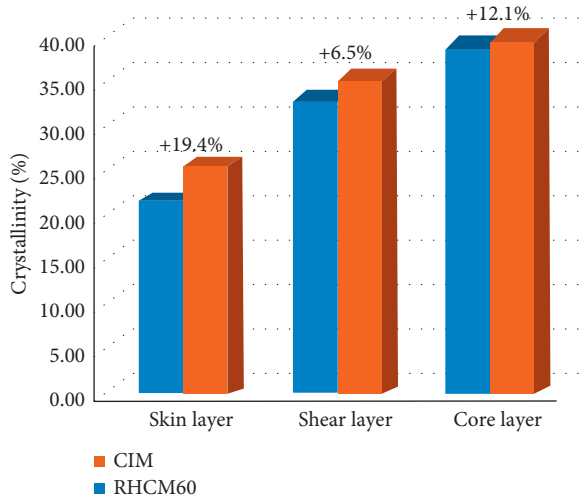

(c)

Figure 11: Comparison of microstructure layers in RHCM60 and CIM samples: (a) depth; (b) fiber orientation tensor; (c) crystallinity.

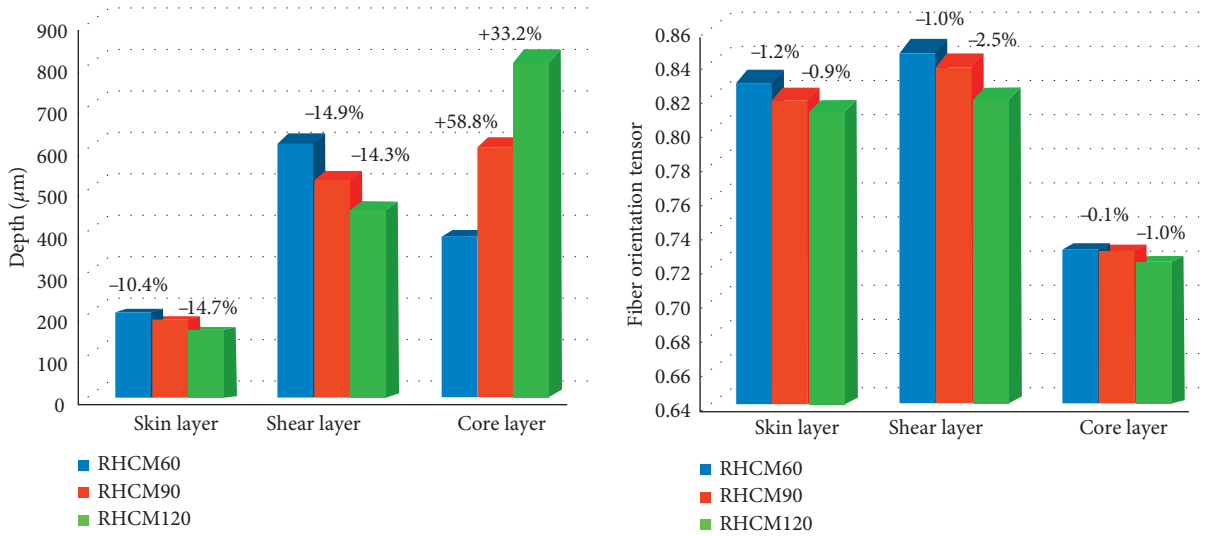

(a) (b)

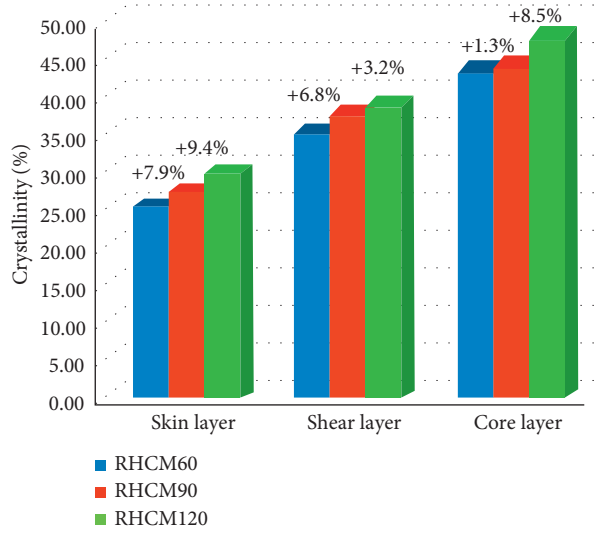

(c)

Figure 12: Comparison of microstructure layers in RHCM samples. (a) depth; (b) fiber orientation tensor; (c) crystallinity.

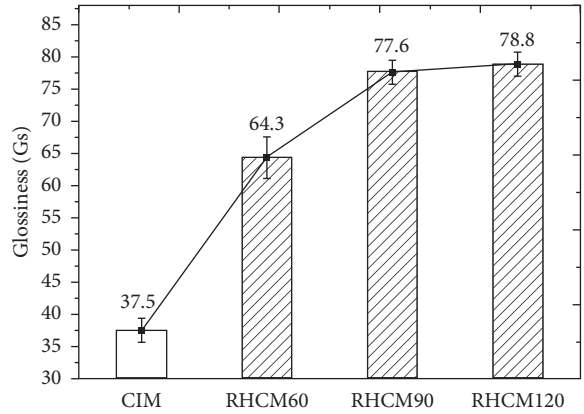

Figure 13: Glossiness variance trends of samples molded at different cavity surface temperatures.

Table 2: Surface roughness of test samples.

Roughness	Ra (μm)					Average
Sample	1	2	3	4	5	
CIM	0.944	1.042	0.668	0.636	0.895	0.837
RHCM60	0.352	0.431	0.336	0.337	0.358	0.363
RHCM90	0.181	0.234	0.212	0.189	0.216	0.206
RHCM120	0.196	0.235	0.190	0.213	0.155	0.198

of the sample can be effectively improved by increasing the mold surface temperature. In the RHCM process, as the mold cavity surface temperature increases, the number of exposed surface fibers decreases because the fluidity of the polymer in the skin layer is enhanced. It is easier for the polymer melt to fill in the gap formed between the fiber and cavity surface, and the fiber of the skin layer can be well-wrapped by the polymer matrix without being exposed outside the skin layer.

Figure 14 shows the microsurface images of GFRPP samples molded at different cavity surface temperatures immediately before filling. With the temperature rising, a smooth mold surface can be accurately reproduced; hence, the surface roughness of the product is gradually decreased. The greater the surface roughness, the larger the undulation of the microscopic surface of the product and the stronger the scattering of light; this means that the gloss of the product becomes lower with the increase in surface roughness. Figure 14 further shows that the surface gloss increase is not distinct after the surface temperature reaches 90°C; this phenomenon is consistent with results found by Wang et al. [33]. They attributed this high gloss surface to the amorphous phase, which completely wrapped all crystalline phases on the surface; finally, the surface presented a pure and uniform amorphous phase. However, this conclusion differs from the observations of other researchers [17, 21, 31] who indicated that the surface of the PP sample is composed of both crystalline and amorphous phases. Another researcher (Wang et al. [35]) pointed out that, for the virgin PP, the surface gloss exhibited a different trend: instead of increasing, it tended to decrease as the cavity surface temperature continued to rise after reaching 110°C.

To better comprehend the mechanism involved in attaining the best gloss quality exhibited by RHCM120, WAXRD technology is employed to estimate the surface crystallization. The WAXRD patterns of RHCM90 and RHCM120 are shown in Figure 15. Note that the orientation parameters of these two samples are practically the same; however, the surface crystallinity of RHCM120 is relatively higher than that of RHCM90. This is because the higher mold surface temperature not only substantially increases the surface crystallization rate of the product, but also increases the crystallization time; thus, the crystallinity on the surface of RHCM120 is relatively high. The high surface crystallinity indicates that the surface crystal area is large, and the molecular chains on the surface are regularly arranged; this can effectively suppress light scattering and thereby improve surface gloss.

The foregoing analysis indicates that when the mold heating temperature is below 90°C, the increase in the surface gloss of the sample is mainly because of the reduction in the surface-exposed floating fibers and the improvement in the melt surface replication ability. When the cavity surface temperature is more than 90°C, the surface gloss increase is primarily attributed to the increase in surface crystallinity combined with the higher surface replication ability of the melt.

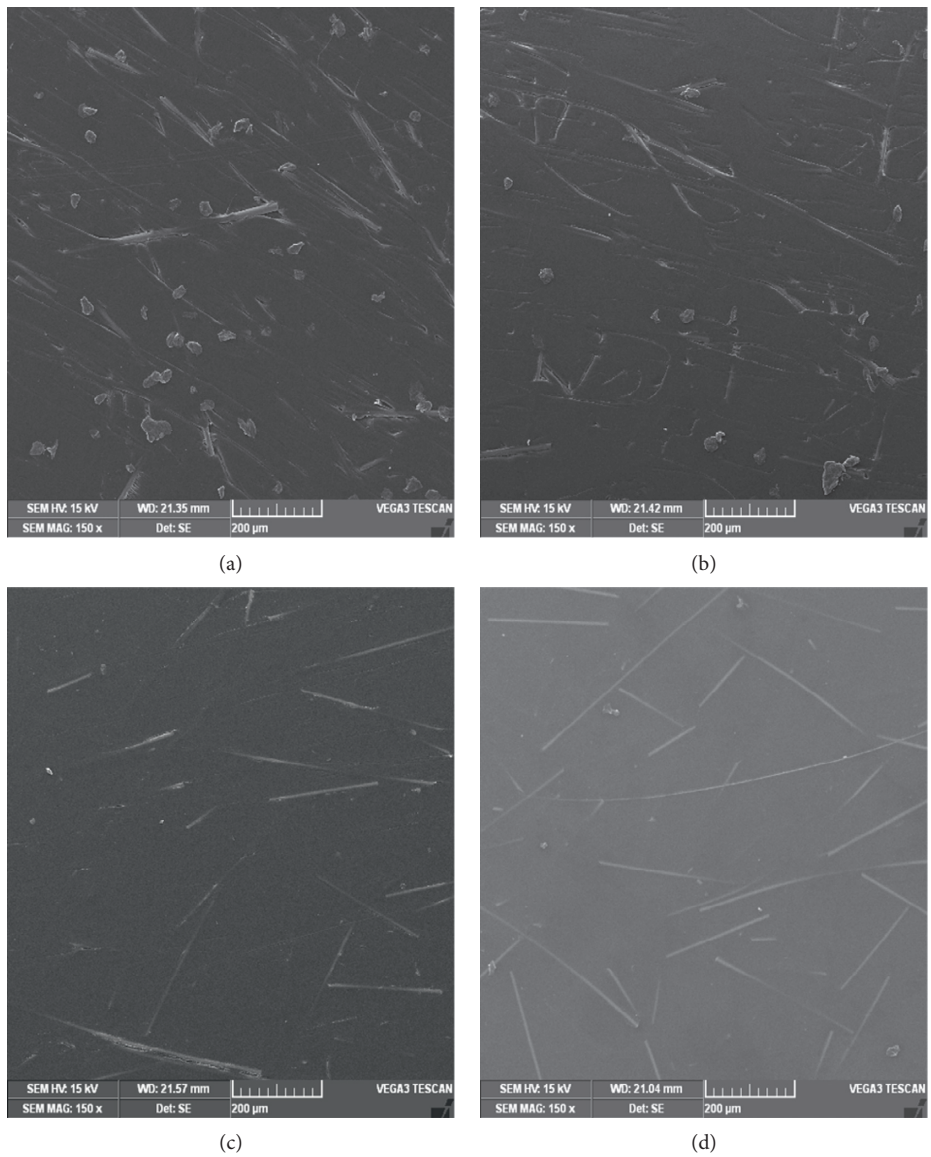

Figure 14: Microsurface images of GFRPP samples molded at different cavity surface temperatures immediately before filling: (a) CIM; (b) RHCM60; (c) RHCM90; (d) RHCM120.

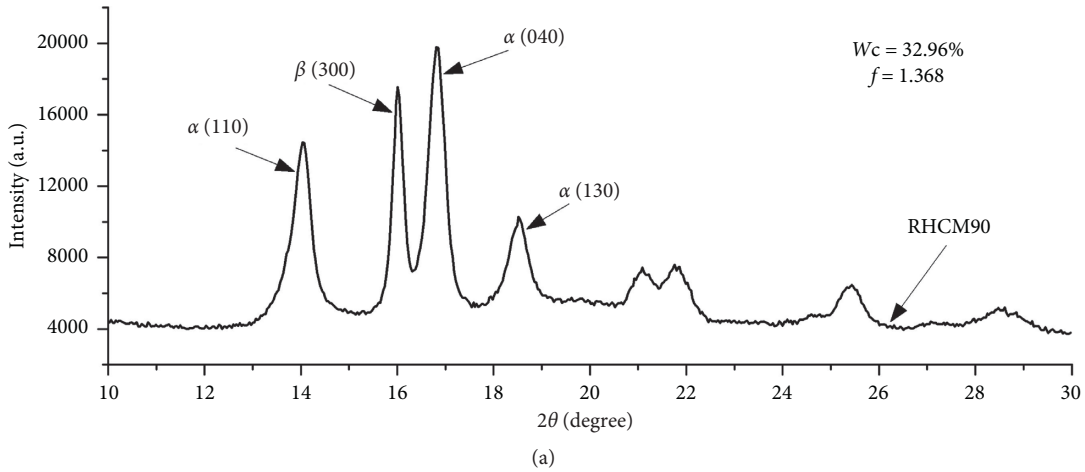

Figure 15: Continued.

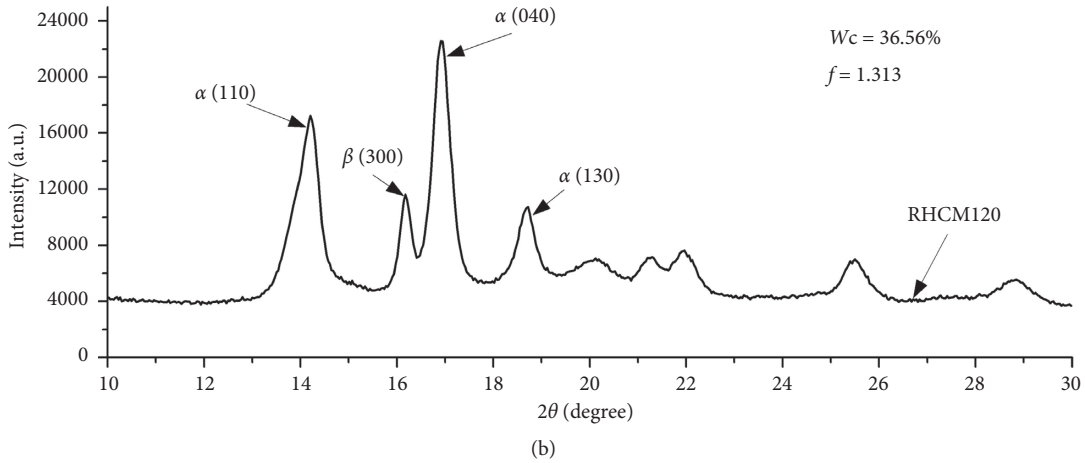

Figure 15: X-ray diffraction curves of (a) RHCM90 and (b) RHCM120.

4. Conclusions

In this study, the effect of mold cavity surface temperature on the tensile and surface gloss properties is investigated in 30% short glass fiber-reinforced PP composites without weld lines. The influence mechanisms of temperature are discussed and revealed by coupling simulation, SEM, WAXRD, DMA, roughness meter, and surface gloss meter. The corelationship between the macroscopic properties (tensile strength and surface gloss), microstructure, and processing of RHCM samples are discussed. The main conclusions drawn are as follows.

(1) The tensile strength first increases and then decreases as the cavity surface temperature increases before filling. RHCM60 sample has the highest tensile strength followed by RHCM90 and CIM samples; RHCM120 sample has the lowest tensile strength. These differences are mainly because the microstructure of GFRPP composites considerably depends on the preassigned cavity surface temperature.

(2) With increasing cavity surface temperature before filling, the thickness of skin layer with a medium fiber orientation along the flow direction decreases continuously. The thickness of the shear layer with a strong fiber orientation first increases and then decreases, and all the shear layers of RHCM samples are thicker than that of the CIM sample; RHCM60 sample has the widest shear layer thickness. The thickness of the core layer with a weak fiber orientation first decreases and thereafter increases; RHCM120 and RHCM60 samples have the thickest and thinnest core layers, respectively.

(3) Each layer fiber orientation in all samples exhibits an increasing and thereafter decreasing trend with increasing cavity surface temperature. Each layer fiber orientation in RHCM60 sample is higher than that in the CIM sample. The crystallinity in each layer in all samples increases with increasing cavity surface temperature, and the same variance trend can be observed between the fiber-matrix interfacial bonding strength in all samples and cavity surface temperature.

(4) The sample surface gloss increases with the increase in the surface temperature of the mold cavity; however, when the temperature exceeds 90°C, the growth trend sharply slows down. Moreover, among all samples, the surface crystallinity in RHCM120 sample is the highest. When the mold heating temperature is lower than 90°C, the increase in surface gloss is mainly attributed to the reduction in the exposed floating fiber and the enhancement of the melt surface replication ability. When the mold heating temperature is more than 90°C, the surface gloss increases mainly because of the increase in the surface crystallinity coupled with the high level of the mirror surface replication ability of the melt.

Data Availability

All data used to support the findings of this study are included with the article.

Conflicts of Interest

The authors declare that there are no conflicts of interest regarding the publication of this paper.

Acknowledgments

The authors acknowledge the financial support of the Zhejiang Provincial Natural Science Foundation of China (Grant nos. LY19E050004 and LY19E050009), the National Natural Science Foundation of China (Grant nos. 51575491 and U1610112), and the Zhejiang Provincial Department of Education Foundation of China (Grant no. Y201737711).

References

[1] A. R. Albooyeh, "The effect of addition of Multiwall Carbon Nanotubes on the vibration properties of Short Glass Fiber

reinforced polypropylene and polypropylene foam composites," *Polymer Testing*, vol. 74, pp. 86–98, 2019.

[2] K. Friedrich and A. A. Almajid, "Manufacturing aspects of advanced polymer composites for automotive applications," *Applied Composite Materials*, vol. 20, no. 2, pp. 107–128, 2013.

[3] G. Colucci, H. Simon, D. Roncato, B. Martorana, and C. Badini, "Effect of recycling on polypropylene composites reinforced with glass fibres," *Journal of Thermoplastic Composite Materials*, vol. 30, no. 5, pp. 707–723, 2017.

[4] H. Ikbal, Q. Wang, A. Azzam, and W. Li, "GF/CF hybrid laminates made through intra-tow hybridization for automobile applications," *Fibers and Polymers*, vol. 17, no. 9, pp. 1505–1521, 2016.

[5] E. I. Kurkin and V. O. Sadykova, "Application of short fiber reinforced composite materials multilevel model for design of ultra-light aerospace structures," *Procedia Engineering*, vol. 185, pp. 182–189, 2017.

[6] R. S. Bay, *Fiber Orientation in Injection-Molded Composites: A Comparison of Theory and Experiment*, St Edmundsbury Press, Suffolk, UK, 1991.

[7] S. Liparoti, A. Sorrentino, V. Speranza, and G. Titomanlio, "Multiscale mechanical characterization of iPP injection molded samples," *European Polymer Journal*, vol. 90, pp. 79–91, 2017.

[8] Z. Wang, G. Zheng, B. Wang et al., "Suppressing the skin-core structure in injection-molded HDPE parts via the combination of pre-shear and UHMWPE," *RSC Advances*, vol. 5, no. 103, pp. 84483–84491, 2015.

[9] X. P. Li, N. N. Gong, Z. Gao et al., "Fiber orientation in melt confluent process for reinforced injection molded part," *International Journal of Advanced Manufacturing Technology*, vol. 90, no. 5–8, pp. 1457–1463, 2017.

[10] C. Kahl, M. Feldmann, P. Sälzer, and H.-P. Heim, "Advanced short fiber composites with hybrid reinforcement and selective fiber-matrix-adhesion based on polypropylene—characterization of mechanical properties and fiber orientation using high-resolution X-ray tomography," *Composites Part A: Applied Science and Manufacturing*, vol. 111, pp. 54–61, 2018.

[11] J. L. Thomason and G. E. Schoolenberg, "An investigation of glass fibre/polypropylene interface strength and its effect on composite properties," *Composites*, vol. 25, no. 3, pp. 197–203, 1994.

[12] J. Hou, G. Zhao, G. Wang, G. Dong, and J. Xu, "A novel gas-assisted microcellular injection molding method for preparing lightweight foams with superior surface appearance and enhanced mechanical performance," *Materials & Design*, vol. 127, pp. 115–125, 2017.

[13] E. Haberstroh and H. Wehr, "Rubber processing with gas-assisted injection moulding (R-GAIM)," *Macromolecular Materials and Engineering*, vol. 284-285, no. 1, pp. 76–80, 2000.

[14] X. H. Liu, Y. M. Pan, G. Q. Zheng et al., "Overview of the experimental trends in water-assisted injection molding," *Macromolecular Materials & Engineering*, vol. 303, no. 8, pp. 1–13, 2018.

[15] D. Mi, R. La, T. Wang, X. Zhang, and J. Zhang, "Hierarchic structure and mechanical property of glass fiber reinforced isotactic polypropylene composites molded by multiflow vibration injection molding," *Polymer Composites*, vol. 38, no. 12, pp. 2707–2717, 2017.

[16] D. Yao, S.-C. Chen, and B. H. Kim, "Rapid thermal cycling of injection molds: an overview on technical approaches and applications," *Advances in Polymer Technology*, vol. 27, no. 4, pp. 233–255, 2008.

[17] G. L. Wang, G. Q. Zhao, and Y. J. Guan, "Thermal response of an electric heating rapid heat cycle molding mold and its effect on surface appearance and tensile strength of the molded part," *Journal of Applied Polymer Science*, vol. 128, no. 3, pp. 1339–1352, 2013.

[18] S.-C. Chen, Y.-W. Lin, R.-D. Chien, and H.-M. Li, "Variable mold temperature to improve surface quality of microcellular injection molded parts using induction heating technology," *Advances in Polymer Technology*, vol. 27, no. 4, pp. 224–232, 2008.

[19] S. Liparoti, A. Sorrentino, G. Guzman, M. Cakmak, and G. Titomanlio, "Fast mold surface temperature evolution: relevance of asymmetric surface heating for morphology of iPP molded samples," *RSC Advances*, vol. 5, no. 46, pp. 36434–36448, 2015.

[20] L. Crema, M. Sorgato, F. Zanini, S. Carmignato, and G. Lucchetta, "Experimental analysis of mechanical properties and microstructure of long glass fiber reinforced polypropylene processed by rapid heat cycle injection molding," *Composites Part A: Applied Science and Manufacturing*, vol. 107, pp. 366–373, 2018.

[21] Z. Shayfull, S. Sharif, A. M. Zain et al., "Potential of conformal cooling channels in rapid heat cycle molding: a review," *Advances in Polymer Technology*, vol. 33, no. 1, pp. 725–738, 2014.

[22] J. Li, T. Li, Y. Jia, S. Yang, S. Jiang, and L.-S. Turng, "Modeling and characterization of crystallization during rapid heat cycle molding," *Polymer Testing*, vol. 71, pp. 182–191, 2018.

[23] W. H. Wang, G. Q. Zhao, Y. J. Guan et al., "Effect of rapid heating cycle injection mold temperature on crystal structures, morphology of polypropylene and surface quality of plastic parts," *Journal of Polymer Research*, vol. 22, no. 5, pp. 1–11, 2015.

[24] V. Speranza, S. Liparoti, R. Pantani, and G. Titomanlio, "Hierarchical structure of iPP during injection molding process with fast mold temperature evolution," *Materials*, vol. 12, no. 3, p. 424, 2019.

[25] S. Liparoti, A. Sorrentino, and G. Titomanlio, "Rapid control of mold temperature during injection molding process: effect of packing pressure," *American Institute of Physics*, vol. 1965, pp. 0200521–0200524, 2015.

[26] G. Wang, G. Zhao, and X. Wang, "Effects of cavity surface temperature on reinforced plastic part surface appearance in rapid heat cycle moulding," *Materials & Design*, vol. 44, pp. 509–520, 2013.

[27] G. Wang, G. Zhao, and X. Wang, "Effects of cavity surface temperature on mechanical properties of specimens with and without a weld line in rapid heat cycle molding," *Materials & Design*, vol. 46, pp. 457–472, 2013.

[28] J. Li, W. Zheng, S. Jiang, and G. Chai, "An experimental study of skin layer in rapid heat cycle molding," *Polymer-Plastics Technology and Engineering*, vol. 53, no. 5, pp. 488–496, 2014.

[29] X. P. Li, G. Q. Zhao, and C. Yang, "Effect of mold temperature on motion behavior of short glass fibers in injection molding process," *International Journal of Advanced Manufacturing Technology*, vol. 73, no. 5–8, pp. 639–645, 2014.

[30] Y. G. Zhou, B. Su, and L. S. Turng, "Mechanical properties, fiber orientation, and length distribution of glass fiber-reinforced polypropylene parts: influence of water-foaming technology," *Polymer Composites*, vol. 39, no. 12, pp. 4368–4399, 2018.

[31] H. B. H. Salah, H. B. Daly, J. Denault, and F. Perrin, "Morphological aspects of injected polypropylene/clay nanocomposite materials," *Polymer Engineering & Science*, vol. 53, no. 5, pp. 905–913, 2013.

[32] M. A. Kashfipour, N. Mehra, and J. H. Zhu, "A review on the role of interface in mechanical, thermal, and electrical properties of polymer composites," *Advanced Composites & Hybrid Materials*, vol. 1, no. 3, pp. 415–439, 2018.

[33] G. L. Wang, G. Q. Zhao, and X. X. Wang, "Experimental research on the effects of cavity surface temperature on surface appearance properties of the moulded part in rapid heat cycle moulding process," *International Journal of Advanced Manufacturing Technology*, vol. 68, no. 5–8, pp. 1293–1310, 2013.

[34] L. A. Pothan, Z. Oommen, and S. Thomas, "Dynamic mechanical analysis of banana fiber reinforced polyester composites," *Composites Science and Technology*, vol. 63, no. 2, pp. 283–293, 2003.

[35] M. H. Wang, J. J. Dong, W. H. Wang et al., "Optimal design of medium channels for water-assisted rapid thermal cycle mold using multi-objective evolutionary algorithm and multi-attribute decision-making method," *International Journal of Advanced Manufacturing Technology*, vol. 68, no. 9–12, pp. 2407–2417, 2013.